Influence of Deformation-Induced alpha prime Martensite on the Crack Initiation Mechanism in a Metastable Austenitic Steel in the HCF and VHCF Regime

Martina Zimmermann[1,*], A. Grigorescu[2], C. Müller-Bollenhagen[3], H.-J. Christ[2]

[1] Institut für Werkstoffwissenschaft, Technische Universität Dresden, Dresden 01062, Germany
[2] Institut für Werkstofftechnik, Universität Siegen, Siegen 57068, Germany
[3]Continental Teves AG & Co. oHG, Hannover 30419, Germany
* Corresponding author: martina.zimmermann@tu-dresden.de

Abstract
Fatigue failure in the VHCF regime of high strength steels is dominated by subsurface crack initiation around non-metallic inclusions with fisheye fracture morphology. However, this unique failure mechanism cannot be thoroughly confirmed for metastable austenitic steel 1.4301 (AISI 304), for its crack origin is heavily dependant on fatigue life and its amount of deformation-induced alpha prime martensite. In the HCF regime cracks originate at the specimen surface from inclusions exceeding 0.02 mm, irrespective of the volume fraction of deformation-induced alpha prime martensite. For a volume fraction beyond $V_M = 30\%$ the higher notch sensitivity of the martensite phase can lead to crack initiation at micro flaws at the surface. In the VHCF regime the influence of the martensite content is even more dominant, as for $V_M = 54\%$ the crack origin shifts to subsurface inclusions. While the formation of a fine granular area is observed for all cases with $V_M > 50\%$, the occurrence of a typical fisheye morphology depends on the inclusion's relative position to the specimen's surface. The diversity of crack initiation mechanisms can be explained by the interaction of the austenite and martensite phases and its different ductilities with the inclusions as shown by TEM micrographs and Murakami's model of hydrogen-induced VHCF failure.

Keywords
Very high cycle fatigue, metastable austenitic steel, deformation induced martensite, fisheye fracture

1. Introduction

In recent years, many investigations (e.g. [1,2]) focused on the diversity of damage mechanisms related to failure beyond the classical fatigue limit, i.e. at a number of loading cycles $N > 10^7$. At an early stage of research on the fatigue of materials in the very high cycle range, a distinction between single phase and defect free type I materials and multiphase type II materials with microstructural defects such as non-metallic inclusions or pores was proposed by Mughrabi [3,4]. The discussion about the fatigue behaviour of the two types of materials at very high number of cycles and the underlying damage mechanisms is often combined with hypotheses of the course of the S–N curve such as a duality of the curve related to the crack initiation position [5,6]. For type II materials a multistage S–N curve is defined by the change from surface crack initiation to a control of fatigue life by crack nucleation at internal defects. With regard to high strength steels, different models for damage mechanisms and the multistage S-N curve are currently under discussion.

Murakami et al. [7] related the formation of a so-called fisheye fracture surface, which is commonly observed in these types of materials in the VHCF range, to a hydrogen embrittlement due to a hydrogen concentration in the vicinity of inclusions. According to Murakami and Endo, the VHCF behavior can be correlated to the size and hardness of nonmetallic inclusions [8]. A different explanation was suggested by Sakai et al. [9] stating that the fisheye formation by means of the formation of a fine granular layer around the inclusion is a consequence of a nucleation and coalescence of microdebondings. The formation of fisheye fractures due to multiple microcracks initiated by the decohesion of spherical carbides from the matrix around the dominating inclusion is given as the major damage mechanism model by Shiozawa et al. [10]. This model was confirmed

by the findings of Sohar et al. for a high Cr alloyed cold worked tool steel, where internal as well as near surface fisheye fracture was observed in the VHCF regime and attributed to the formation and coalescence of microcracks around carbide clusters [11]. Despite these findings not all steels containing nonmetallic inclusions can be classified in one of the given models. Results for the HCF and VHCF behavior of a metastable austenitic stainless steel presented in this paper demonstrate that both the actual cyclic strength of a material, the course of the S–N curve and the underlying damage mechanisms are highly sensitive to microstructural changes.

2. Material and Experimental Methods

The material chosen for this study was a solution annealed metastable austenitic stainless steel sheet AISI304 (1.4301) with a thickness of 2 mm. Its chemical composition determined by means of spectral analysis is given in table 1. A relatively low stability of the austenite phase is caused by the low amount of nickel in the overall alloy composition. The deformation induced α' martensite content was regulated by a one-step predeformation carried out by means of a servohydraulic test system equipped with a liquid nitrogen-cooled chamber, allowing a deformation start temperature of -100°C. Before fatigue testing, all specimens were mechanically and subsequently electro-chemically polished but for several reference specimens with artificial micronotches at the surface. For the fatigue experiments two testing systems were used: a resonance pulsation test stand operating at ~ 90 Hz and an ultrasonic fatigue testing system working at a frequency of ~ 20 kHz. All fatigue experiments were executed in a fully reversed mode under load control. Specimens' heating was averted by cooling with compressed air and in addition by a pulse-pause testing mode for the ultrasonic system. The alpha prime martensite volume fraction was measured by means of a magneto-inductive testing device (Fischer feritscope).

The characterization of microstructure and the fractographic analysis of the fatigued samples were accomplished by means of a scanning electron microscope (FEI, Helios) equipped with an ion source which permits a selective removal of lamellae for transmission electron microscopy (Hitachi).

Table 1. Chemical composition of the alloying elements for AISI304 analysed by means of spectral analysis.

C	Si	Mn	P	S	Cu	Cr	Mo	Ni	V	N
0,024	0,43	1,43	0,021	0,007	0,14	18,3	0,038	8,11	0,1	0,067

3. Results

3.1 Fatigue behavior

Fatigue results are given in figure 1a, open symbols indicate samples that were solely tested with the resonance system up to 10^8 cycles while crossed symbols represent samples fatigued firstly with the resonance pulsation system up to cyclic saturation and subsequently with the ultrasonic system. In the fully austenitic condition the metastable austenitic steel studied exhibits a constant fatigue limit of 250 Pa in the HCF and the VHCF region. No failure happened even up to a number of loading cycles $N > 10^8$. A true durability for $N > 10^6$ cycles for AISI304 in the fully austenitic condition is confirmed by various authors [12-15] except for the work by Bathias [16], who observed failure in the VHCF regime for this steel type. In the fully austenitic condition the material's fatigue behavior is dominated by a strong transient behavior with a pronounced cyclic softening up to $N \sim 10^5$ followed by cyclic hardening up to 2×10^7 cycles. More details of the correlation between the cyclic deformation behavior of the material presented and its resonance behavior is given in [17]. The cyclic hardening can be explained by a martensite formation which

results in a decrease of the strain amplitude. Hence, the global loading situation declines well below a threshold value for irreversible slip activities so that the fatigue limit can be regarded as a true infinite durability for the fully austenitic condition. However, the martensite formation during cyclic loading in the VHCF regime is quite surprising as the plastic strain amplitude (3×10^{-4}) is well below the threshold value for martensite formation of 3×10^{-3} according to literature.

The fatigue behavior of specimens in the one-step predeformed condition displays a steady increase of cyclic strength in the HCF regime with increasing volume fraction of deformation induced martensite (Figure 1a). At the same time the disposition to a transient behavior during cyclic deformation fades. For the HCF regime the fatigue limit increases with increasing martensite volume fraction. However, this is only true for specimens with a well preserved surface without flaws and defects. In case of artificial micro notches (with a depth of 12 up to 40 µm) at the surface a peak cyclic strength could be identified for a volume fraction of α' martensite $\leq 30\%$. A comparison of actively cooled and uncooled fatigue tests demonstrate the influence of α' martensite formation on the cyclic strength during testing. The lack of active cooling prevents the formation of α' martensite and as a consequence lowers the cyclic strength drastically (figure 1b).

For the VHCF regime a change in the fatigue behavior can be observed with increasing volume fraction of alpha prime martensite. For a volume fraction of 54% failure occurs even beyond the classical fatigue limit resulting in a two-step S-N-curve with crack initiation up to a number of loading cycles $N > 10^8$. Therefore it stands to reason that a change in damage mechanism due to the degree of phase transformation is inherent for AISI304. This phenomenon can be explained by the metallographic analysis presented in the subsequent chapter.

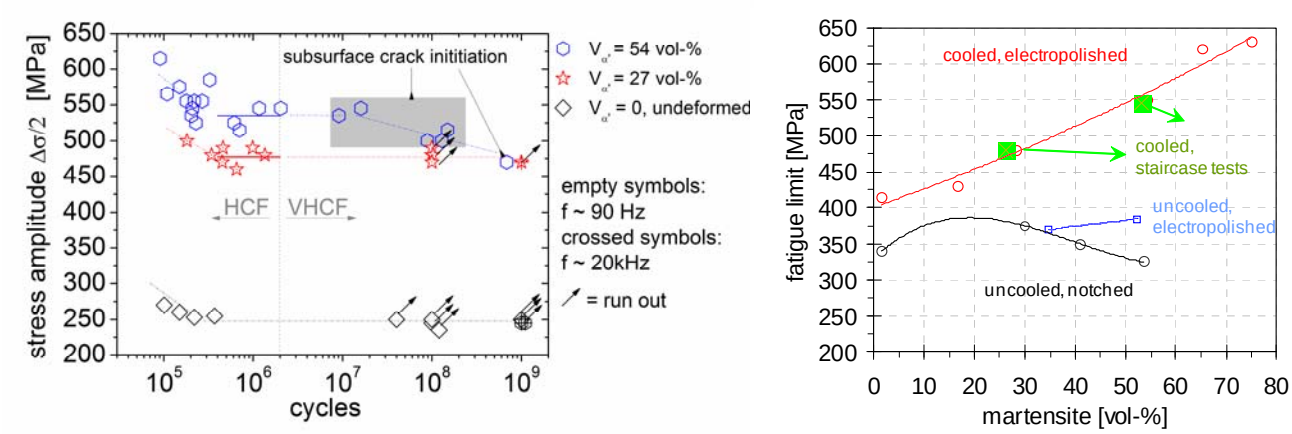

a) b)

Figure 1: Fatigue behavior in the HCF and VHCF regime (a) and comparison of fatigue limit for the HCF region related to different testing conditions and samples with artificial micro notches (b).

3.2 Damage mechanisms

The fatigue behavior of AISI304 in the fully austenitic condition is characterized by two major microstructural processes: inhomogeneously distributed strain localization in narrow slip bands and formation of α' martensite at intersections of slip bands as well as formation of martensite needles (figure 2). The phase transformation leads to a decrease of dislocation mobility and hence to an increase in cyclic strength and a true durability in the VHCF regime. Fractographic analysis of the specimens tested and failed in the HCF region (here: failure only for $N < 10^6$) reveal the importance of microstructural flaws and defects at or near the specimens surface. All failures in the HCF regime can be attributed to crack initiation at nonmetallic inclusions in the near-surface region (figure 3a).

However, inclusions with a size up to 20 µm did not result in HCF failure. In contrast, artificial micro notches at the surface are the reason for a decline of the fatigue strength in the HCF region for higher α' martensite volume fractions (figure 3b), which can be ascribed to the higher notch sensitivity of the martensite phase. According to Bowe et al. [18] the threshold value for fatigue crack growth for the fully austenitic condition of a FeNiAl-alloy is five times higher than that for the martensitic condition. It can therefore be assumed, that a higher amount of martensite phase enclosing a surface defect results in an earlier crack initiation and accelerated crack growth.

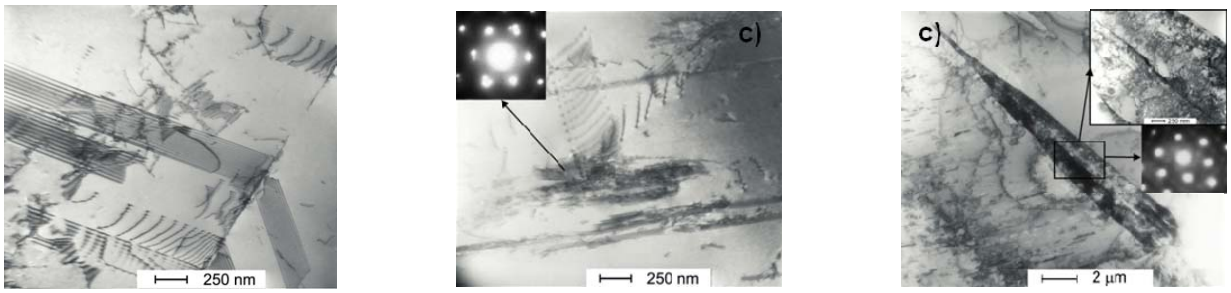

a) b) c)

Figure 2: Formation of slip bands (a), α' martensite in the bulk at slip band intersections (b) and a martensite needle (c) during cyclic loading at σ = 240 MPa and N = 10^7.

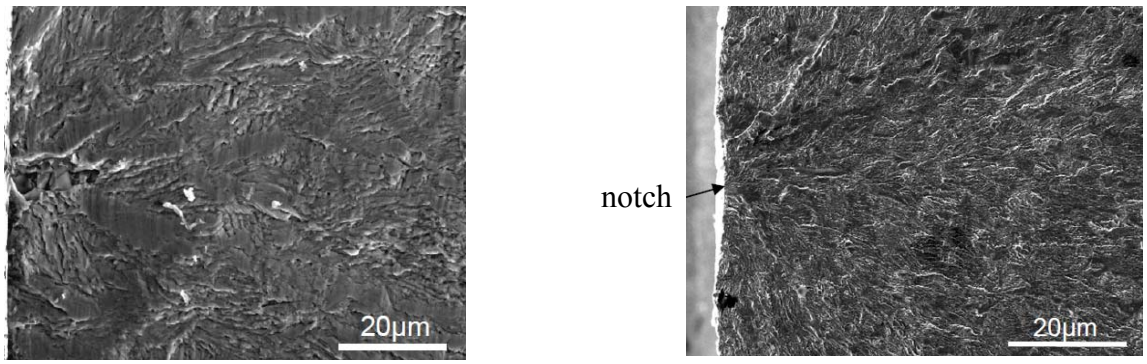

a) b)

Figure 3: Crack initiation in the HCF region at a surface inclusion for a specimen with 27% α' martensite volume fraction (a) and at an artificial micro notch for 30% α' martensite volume fraction (b).

A one-step predeformation leads to a pronounced increase of the cyclic strength for AIS304, but at the same time to failure even in the VHCF regime for an α' martensite volume fraction of 54%. This change in damage mechanism can be explained by comparing the microstructure of the fully austenitic with the predeformation condition. The major difference lies in the amount and distribution of α' martensite. For a volume fraction of 27% the α' martensite is loosely allocated at slip band intersections (figure 4a) and the local notch stress around an inclusion leads to a concentration of the deformation in the softer austenite phase (represented for a fully austenitic condition in figure 4c) and a formation of deformation induced martensite. The localized work hardening and the compression stresses due to phase transformation impede crack initiation at the inclusion. Interconnected clusters of α' martensite dominate the microstructure for a volume fraction of 56% (figure 4b). Due to the coherency of the martensite clusters, the deformation is no longer compensated by the softer austenite phase and the low ductility of the martensite phase results in crack initiation even at stress amplitudes in the VHCF range. Figure 5 depicts an example for crack initiation at an elongated inclusion for a sample with a volume fraction of martensite > 30%. The crack starts in the austenite phase leading to a brittle fracture of the inclusion before propagating into the notch-sensitive martensite phase. This example demonstrates that an inclusion does not necessarily have to be completely surrounded by the martensite phase. Elastic deformation in the martensitic phase might already be sufficient to have a crack initiating effect in the austenitic

phase in the vicinity of an inclusion.

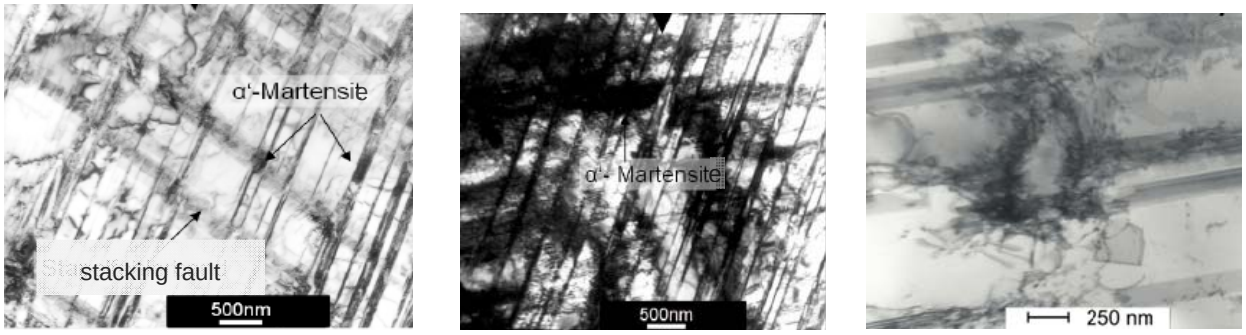

a) b) c)

Figure 4: Phase morphology after the formation of predeformation-induced α' martensite with a volume fraction of 27% (a) and of 54% (b) produced by different deformation start temperatures and dislocation coalescence around an inclusion (c).

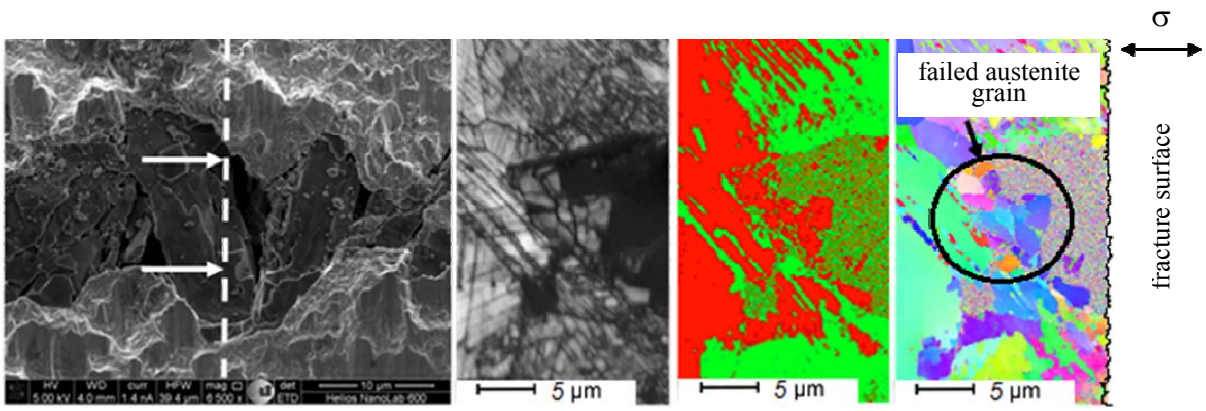

a) b) c) d)

Figure 5: Crack initiation at an inclusion (a), image quality of the inclusion in the direction perpendicular to the fracture surface (b), phase distribution around the inclusion (c) with red = austenite phase and green = martensite phase and inverse pole figure of the inclusion and its surrounding matrix (d).

The VHCF failure for AISI304 with a volume fraction of α' martensite > 30% is accompanied by a change of the crack initiation site from the surface to the specimen interior irrespective of the fact that inclusions encircled by clusters of martensite can also be found in the surface region. The fracture surface of the specimens failed in the VHCF region show a typical fisheye morphology. The crack initiation site is surrounded by a fine granular area (FGA), which according to Sakai [9] is characteristic for the VHCF failure of martensitic steels. The FGA for its part is encompassed by a smooth fracture surface which gives the typical fish-eye appearance. According to Murakami and Matsunaga [19] the cyclic stress intensity factor at the outer front of the FGA can be estimated by

$$\Delta K_{FGA} = 0.5\Delta\sigma\sqrt{\pi\sqrt{area_{FGA}}} \ .$$

An analysis of all specimens' FGAs, which failed in the VHCF regime (figure 1a), result in an average $\Delta K_{FGA} = 4$ MPa√m beiing in good correlation with the threshold value for crack growth of the martensitic phase $\Delta K_{th} = 5$ MPa√m as investigated by Bowe et al. [18]. Hence, the formation of FGA can be regarded as crack initiation phase provided one assumes that the ΔK-concept can be applied for the given VHCF failure mechanism. This phenomenon strongly depends on the number of loading cycles as depicted in figure 6a. There is a steady increase of FGA diameter with increasing number of loading cycles. After reaching a critical value (corresponding to ΔK_{FGA}) a

different crack growth mechanism emerges, developing a rather smooth fracture surface which together with the FGA forms the characteristic fisheye morphology. The cycle dependence of FGA formation explains the dual step S-N-curve (figure 1a). In the VHCF regime a minimum number of cycles is necessary before continuous crack growth in the form of the smooth fisheye fracture surface results in overall failure.

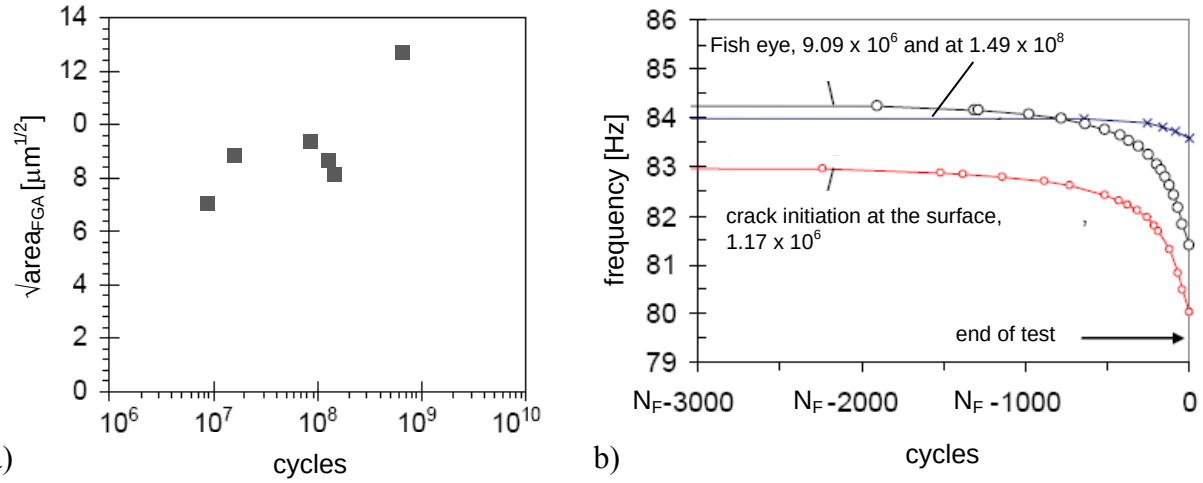

Fig. 6: Correlation between √area of the FGA and number of loading cycles (a) and correlation between fisheye formation and resonance frequency (b).

The smooth fracture surface of the fisheye develops as long as the crack growth is still within the interior of the specimen. Hence, the size of the fisheye fracture is directly correlated to the distance of the crack initiating inclusion to the specimen's surface as is depicted in figure 7 for several fracture surfaces. It is well known that crack growth under vacuum is retarded compared to crack growth in air for the material analyzed [20]. As a consequence, cracks will propagate very slowly since vacuum like conditions are still given while the crack front has not yet reached the surface, but will gain momentum the very moment the crack front touches the surface. A correlation between fisheye diameter (150 µm up to 1000 µm) and a predicted as well as measured change in resonance frequency during fatigue testing (figure 6b) revealed, that the formation of fisheye is limited to 2000-3000 cycles of the overall fatigue life. Hence, the major part of fatigue life in the VHCF regime is dominated by the formation of the FGA.

As the development of a FGA is the fatigue life dominating feature, its formation mechanism should be further discussed. Different assumptions as to the origin of the FGA were presented in the introducing chapter. According to Shiozawa et al. [10] the FGA is formed by a decohesion of finely dispersed carbides in the microstructure. This assumption is not plausible for AISI304 with its negligible carbon content (0.02 mass-%). Neither carbides nor microcracks at carbides could be detected in the FGA environment of the specimens (depicted in figure 7) by means of scanning electron microscopy and EDS-analysis. The suggestion made by Sakai [9], that FGA is formed due to a polygonization of very fine subgrains is yet to be discussed as no pronounced fine grained structure could be detected in the crack initiation region.

Murakami et al. [21] assumed that hydrogen trapped at the inclusion leads to the formation of FGAs due to the higher dislocation mobility in the presence of hydrogen. Hydrogen can lead to accelerated crack propagation in the martensitic phase of a metastable austenitic connected and moreover, the hydrogen diffusion coefficient in martensite is four orders of magnitude higher than that in the austenitic phase. Therefore, the model of hydrogen-assisted crack initiation at an

inclusion is assumed as most likely explanation for the formation of FGAs in AISI304 at VHCF-relevant numbers of cycles. Hence, crack initiation and FGA formation is the consequence of agglomerated hydrogen in the martensitic phase around the inclusion increasing the amount of localized plastic deformation in this particular microstructural region. However, this assumption has to be further discussed as in the study presented no final evidence for hydrogen assisted crack initiation was found. Fatigue crack growth tests simulating the microstructural and testing conditions discussed will be necessary for further clarification.

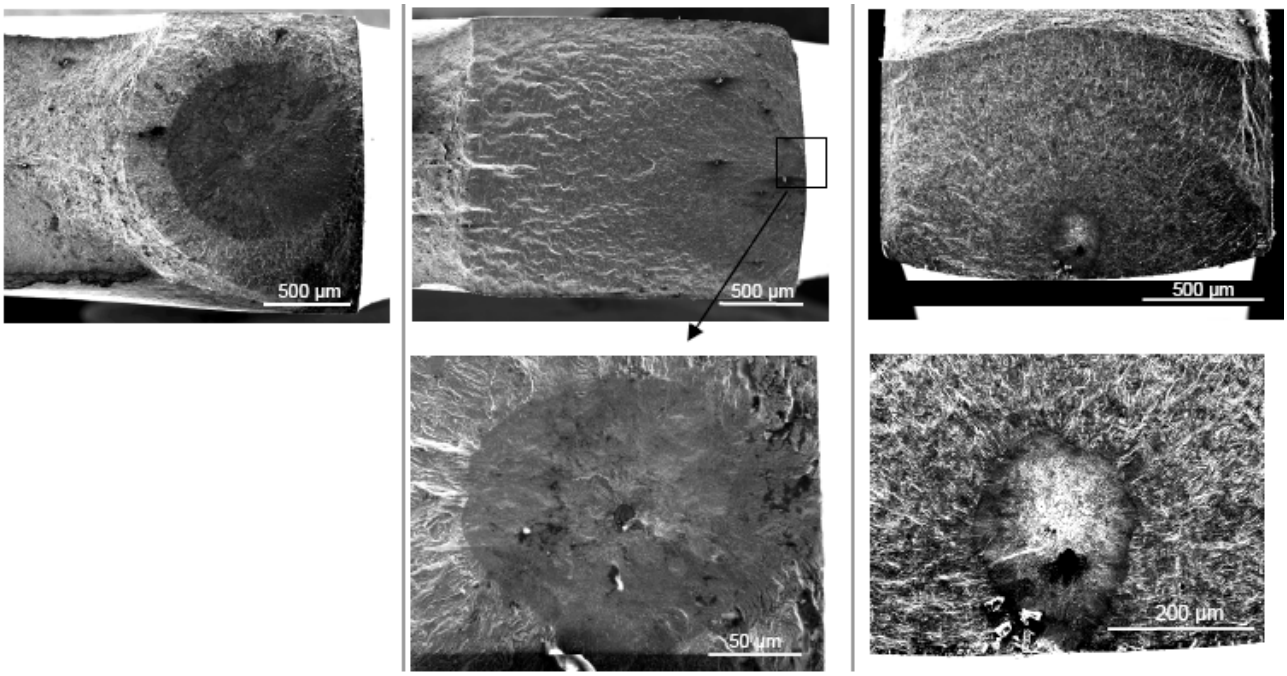

a) b) c)

Fig. 7: Examples for the formation of fisheye fracture morphology with different sizes (depending on the distance between inclusion and specimen surface) a) $\Delta\sigma/2$ = 515 MPa, N_F = 1.49 x 10^8, b) $\Delta\sigma/2$ = 535 MPa, N_F = 9.09 x 10^6 and c) $\Delta\sigma/2$ = 470 MPa, N_F = 6.84 x 10^8.

4. Conclusion

The study presented discusses the change in failure mechanisms of a metastable austenitic steel – an alloy that would typically be classified as material type II with respect to its VHCF behavior – as a function of its volume fraction of deformation-induced α' martensite. In the HCF region AISI304 always failed at inclusions at or very near to the surface, irrespective of its volume fraction of α' martensite. Only surface flaws of a certain size led to earlier failure for a martensite content > 30%. No failure was observed in the VHCF regime for the fully austenitic condition. The VHCF behavior can be explained by the local work hardening of the soft austenitic phase and a very localized phase transformation, both resulting in a decrease of strain amplitude. Hence, the load controlled fatigue tests no longer causes a strain amplitude exceeding a threshold value for crack initiation or microcrack propagation.

In case of an α' martensite volume fraction of 27% a true durability can still be confirmed together with an increase of cyclic strength from ~250 MPa to ~480 MPa compared to the fully austenitic condition. A surface roughening could be observed for the 27% specimens but did not result in crack initiation. However, failure mechanism changes completely with a higher amount of α' martensite volume fraction. A volume fraction of 54-56% leads to a formation of connected

martensite clusters. The localized plastic deformation can no longer be compensated by the softer austenite phase nor will the strain amplitude be reduced due to a local phase transformation. Moreover, it is assumed that hydrogen trapped in the vicinity of inclusions in the specimen's interior increases the dislocation mobility in this region and at the same time promotes the brittleness of the martensitic phase. Inclusions surrounded by such brittle martensite act as local stress raisers and lead to crack initiation in the form of a fine granular area. Fisheye morphology was observed for all specimens that failed in the VHCF regime and the typical smooth fracture surface surrounding the FGA can be explained by crack growth under vacuum-like conditions. A schematic summary of the different failure mechanisms of AISI304 determined for the VHCF behavior is presented in figure 8.

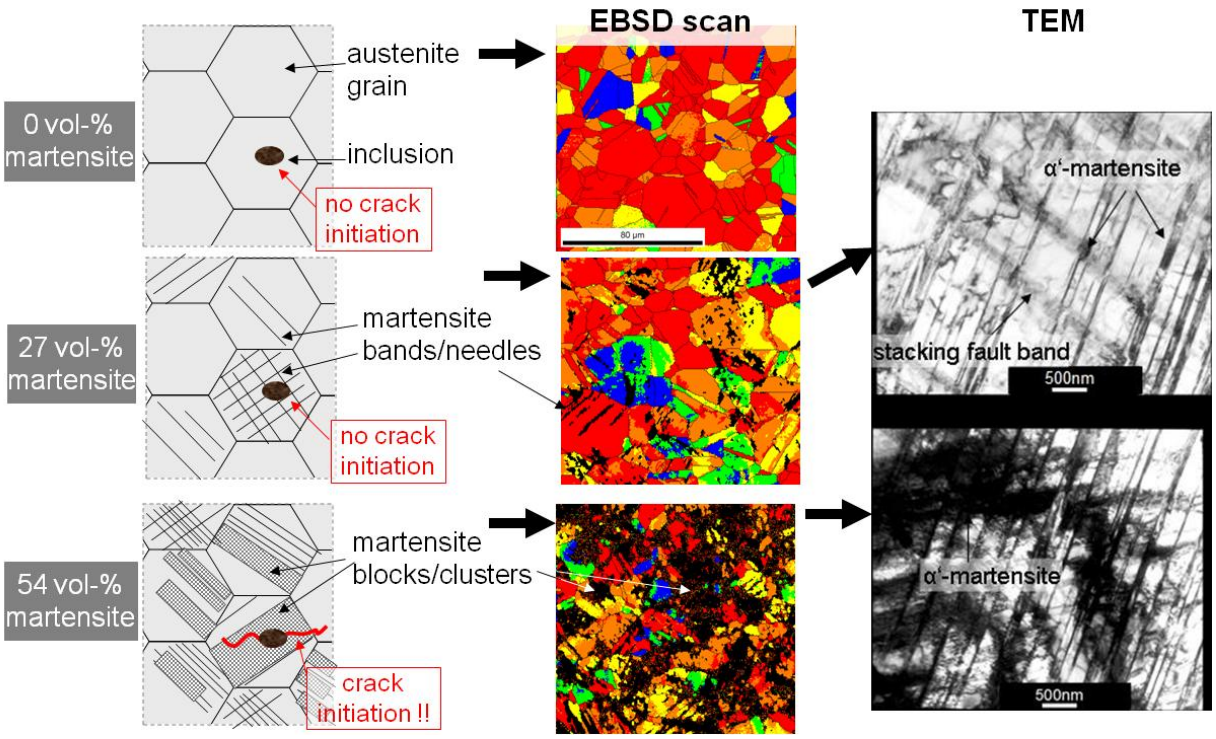

Fig. 8: Change in failure mechanism for VHCF crack initiation in correlation with the volume fraction of α' martensite.

Acknowledgements

The authors gratefully acknowledge the financial support of this study by Deutsche Forschungsgemeinschaft (DFG).

References

[1] M. Zimmermann, Diversity of damage evolution during cyclic loading at very high numbers of cycles – An overview, Int. Mater. Rev., 57 (2012) 73-91.

[2] S. X. Li, Effects of inclusions on very high cycle fatigue properties of high strength steels, Int. Mater. Rev., 57 (2012) 92-114.

[3] H. Mughrabi, Specific features and mechanisms of fatigue in the ultrahigh-cycle regime, Int. J. Fatigue, 28 (2006) 1501-1508.

[4] H. Mughrabi, On 'multi-stage' fatigue life diagrams and the relevant life-controlling mechanisms in ultrahigh-cycle fatigue, Fatigue Fract. Eng. Mater. Struct., 25 (2002)755-764.

[5] S. K. Jha, K. S. R. Chandran, An unusual fatigue phenomenon: duality of the S-N fatigue curve in the β-titanium alloy Ti-10V-2Fe-3Al, Scr. Mater., 48 (2003) 1207-1212.

[6] Y. Murakami, Mechanisms of fatigue failure in ultralong life regime in: S. Stanzl-Tschegg and H. Mayer (Eds), Proc. Int. Conf. on 'Fatigue in the very high cycle range', Vienna, Austria, University of Agricultural Sciences, 2001, pp. 11–22.
[7] Y. Murakami, T. Nomoto, T. Ueda, Factors influencing the mechanism of superlong fatigue failure in steels, Fatigue Fract. Eng. Mater. Struct., 22 (1999) 581–590.
[8] Y. Murakami, M. Endo, Effects of defects, inclusions and inhomogeneities on fatigue strength, Int. J. Fatigue, 16 (1994) 163–182.
[9] T. Sakai, Review and prospects for current studies on very high cycle fatigue of metallic materials for machine structural use, J. Soc. Mech. Eng. Int. J. Ser. A, 3A (2009) 425–439.
[10] K. Shiozawa, Y. Morii, S. Nishino, L. Lu, Subsurface crack initiation and propagation mechanism in high strength steel in a very high cycle fatigue regime, Int. J. Fatigue, 28 (2006) 1521–1532.
[11] C. R. Sohar, A. Betzwar-Kotas, C. Gierl, B. Weiss, H. Danninger, Gigacycle fatigue behavior of a high chromium alloyed cold work tool steel, Int. J. Fatigue, 30 (2008) 2191–2199.
[12] T. H. Myeong, Y. Yamabayashi, M. Shimojo, Y. Higo, A new life extension method for high cycle fatigue using micro martensitic transformation in austenitic stainless steel, Int. J. Fatigue, 19 (1997) 69-73.
[13] T. Nebel, Verformungsverhalten und Mikrostruktur zyklisch beanspruchter metastabiler austenitischer Stähle, Dissertation, 2002, Kaiserlautern.
[14] M. Hayashi, K. Enomoto, Effect of preliminary surface working on fatigue strength of type 304 stainless steel at ambient temperature and 288°C in air and pure water environment, Int. J. Fatigue, 28 (2006) 1626-1632.
[15] M. Nakajima, M. Akita, Y. Uematsu, K. Tokaji, Effect of strain-induced martensitic transformation on fatigue behavior of type 304 stainless steel, Proc. Eng., 2 (2010) 323-330.
[16] C. Bathias, Gigacycle fatigue in mechanical practice, Marcel Dekker, 2005, New York.
[17] P. M. Hilgendorff, A. Grigorescu, M. Zimmermann, C.-P. Fritzen, H.-J. Christ, The effect of damage accumulation in slip bands on the resonant behavior in the very high cycle fatigue (VHCF) regime, Proc. of the 13th Int. Conf. on Fracture, 2013, Beijing.
[18] K. H. Bowe, E. Hammerschmidt, E. Hornbogen, M. Hühner, Bruchmechanische Eigenschaften von metastabilen Austeniten, Materialwiss. Werkstofftech., 19 (1988) 193-201.
[19] Y. Murakami, H. Matsunaga, The effect of hydrogen on fatigue properties of steels used for fuel cell systems, Int. J. Fatigue, 28 (2006) 1509-1520.
[20] A. J. McEvily, J. L. Gonzalez Velazquez, Fatigue crack tip deformation processes influenced by the environment, Metall. Trans., 23A (1992) 2211-2221.
[21] Y. Murakami, T. Nomoto, T. Ueda, On the mechanism of fatigue failure in the superlong life regime ($N > 10^7$ cycles), Part 1: Influence of hydrogen trapped by inclusions, Fatigue Fract. Eng. Mater.Struct., 23 (2000) 893-902.